Pergamon

Geochimica et Cosmochimica Acta, Vol. 68, No. 8, pp. 1749–1761, 2003

0016-7037/03 $30.00 + .00

doi:10.1016/j.gca.2003.07.004

Experimental evidence for carbonate precipitation and CO_2 degassing during sea ice formation

S. PAPADIMITRIOU,[1,*] H. KENNEDY,[1] G. KATTNER,[2] G. S. DIECKMANN,[2] and D. N. THOMAS[1]

[1]University of Wales–Bangor, School of Ocean Sciences, Menai Bridge, Anglesey LL59 5AB, United Kingdom
[2]Alfred Wegener Institute for Polar and Marine Research (AWI), Am Handelshafen 12, D-27570 Bremerhaven, Germany

(*Received January* 24, 2003; *accepted in revised form July* 23, 2003)

Abstract—Chemical and stable carbon isotopic modifications during the freezing of artificial seawater were measured in four 4 m^3 tank incubations. Three of the four incubations were inoculated with a nonaxenic Antarctic diatom culture. The 18 days of freezing resulted in 25 to 27 cm thick ice sheets overlying the residual seawater. The ice phase was characterized by a decrease in temperature from -1.9 to -2.2°C in the under-ice seawater down to -6.7°C in the upper 4 cm of the ice sheet, with a concurrent increase in the salinity of the under-ice seawater and brine inclusions of the ice sheet as a result of physical concentration of major dissolved salts by expulsion from the solid ice matrix. Measurements of pH, total dissolved inorganic carbon (C_T) and its stable isotopic composition ($\delta^{13}C_T$) all exhibited changes, which suggest minimal effect by biological activity during the experiment. A systematic drop in pH and salinity-normalized C_T by up to 0.37 pH_{SWS} units and 376 μmol C kg^{-1} respectively at the lowest temperature and highest salinity part of the ice sheet were coupled with an equally systematic ^{13}C enrichment of the C_T. Calculations based on the direct pH and C_T measurements indicated a steady increase in the in situ concentration of dissolved carbon dioxide (CO_2(aq)) with time and increasing salinity within the ice sheet, partly due to changes in the dissociation constants of carbonic acid in the low temperature–high salinity range within sea ice. The combined effects of temperature and salinity on the solubility of CO_2 over the range of conditions encountered during this study was a slight net decrease in the equilibrium CO_2(aq) concentration as a result of the salting-out overriding the increase in solubility with decreasing temperature. Hence, the increase in the in situ CO_2(aq) concentration lead to saturation or supersaturation of the brine inclusions in the ice sheet with respect to atmospheric pCO_2 ($\approx 3.5 \times 10^{-4}$ atm). When all physico-chemical processes are considered, we expect CO_2 degassing and carbonate mineral precipitation from the brine inclusions of the ice sheet, which were saturated or highly supersaturated with respect to both the anhydrous (calcite, aragonite, vaterite) and hydrated (ikaite) carbonate minerals.

1. INTRODUCTION

Sea ice formation characterizes the polar regions, ranging in extent from 17.5×10^6 to 28.5×10^6 km^2 (Comiso, 2003). At its maximum, sea ice covers 6% of the Earth's surface, thus being one of the largest biomes on earth, similar in size to deserts or the tundra regions (Lizotte, 2001). Sea ice research over the past fifty years has resulted in our understanding of many of the physical processes that transform surface waters into a semisolid state, and the role this has on large scale processes, such as ocean circulation and air-ocean exchange. This has been accompanied by detailed studies of the ecology of sea ice organisms that at times thrive on the ice surfaces or in the labyrinthine brine channel system that permeates sea ice (Thomas and Dieckmann, 2002a). It is only in the past twenty years that there has been any concerted effort into the systematic study of biogeochemical processes in sea ice. These somewhat scant investigations are still frustrated by technological limitations in sampling relevant biogeochemical parameters in the interior of sea ice (Thomas and Dieckmann, 2002b; Thomas and Papadimitriou, 2003). Most recently, interest in sea ice habitats has been stimulated by the prospects of sea ice being a valuable proxy for the conditions that may prevail in extraterrestrial systems, such as on Jupiter's moons, Europa and Ganymede, or on a previously ice-covered Mars (Dieckmann and Hellmer, 2003; Eicken, 2003; Thomas and Dieckmann, 2002a).

A closed sea ice cover results from the coalescing of ice crystals into a loose semisolid phase in the surface of supercooled seawater and their subsequent consolidation upon further freezing into an ice sheet (Eicken, 2003, and references therein). During this process, dissolved salts become concentrated into liquid brine within pockets and channels, which permeate the ice sheet. As the ice sheet thickens and its temperature decreases, the ionic strength of the brine inclusions progressively increases. The quantity of brine enclosed within sea ice is controlled by gravity drainage into the underlying seawater and decreases with time (Eicken, 2003). Brine exchange between the ice sheet and seawater by drainage and convective inflow of seawater may not affect the upper layers of sea ice as they become less permeable and, hence, essentially isolated from external influence with time (Gleitz et al., 1995). Apart from physical brine exchange in younger, more permeable layers of sea ice, solute exchange with seawater is subject to the limitations of molecular diffusion along chemical gradients within the diffusive boundary layer at the ice-seawater interface (Kühl et al., 2001).

The temperature decrease and concomitant dissolved salt enrichment in the brine affect mineral-solution and gas-solution

* Author to whom correspondence should be addressed (s.papadimitriou@bangor.ac.uk).

equilibria (Killawee et al., 1998). Additionally, changes in the dissociation of the weak acids and bases that buffer seawater and influence pH will be prominent as in other hypersaline systems (Lazar et al., 1983). Sequential precipitation of mineral phases is predicted to occur in the range of low temperatures encountered during sea ice formation and growth. Carbonate minerals are the first to precipitate just below the freezing point of seawater (−1.9°C) (Gitterman, 1937; Anderson and Jones, 1985; Marion, 2001). In the absence of biological activity, the temperature decrease and the increased concentration of dissolved constituents in the brine during the freezing of seawater will facilitate supersaturation of dissolved gases with respect to air (Killawee et al., 1998). During the initial stages of ice formation, especially in turbulent water conditions, this will result in the degassing of the brine through nucleation of gas bubbles, which are subsequently trapped within, and become a major feature of the ice matrix (Killawee et al., 1998; Mock et al., 2002).

Carbonate mineral precipitation and degassing of dissolved carbon dioxide can be closely coupled (Usdowski et al., 1979; Clark and Lauriol, 1992; Killawee et al., 1998) and have been well-documented in ice derived from low ionic strength water (Aharon, 1988; Clark and Lauriol, 1992; Fairchild et al., 1993; Killawee et al., 1998). The authigenic carbonate precipitates that form at near-zero and subzero temperatures have been identified as cryogenic calcite and aragonite (op. cit.), while rare occurrences of the metastable forms vaterite (μ-$CaCO_3$) and ikaite ($CaCO_3 \cdot 6H_2O$) have been reported around spring discharges in supraglacial and permafrost environments (Omelon et al., 2001; Grasby, 2003), as well as in low temperature saline lake waters (Bischoff et al., 1993a,b). Mineral precipitation and degassing would appear to be typical, emergent features of sea ice formation and growth, particularly evident in the sea ice dynamics of the dissolved inorganic carbon pool. However, with the exception of the experimental work by Gitterman (1937), observations from natural and artificial sea ice have failed to detect chemical changes commensurate with such processes, and direct observations of authigenic carbonate or other minerals in natural sea ice are scarce (Anderson and Jones, 1985; Gleitz et al., 1995).

Here, we present indirect evidence for carbonate mineral precipitation and CO_2 degassing in artificial sea ice on the basis of the saturation state calculations of seawater and ice brines, using changes in the concentration and the isotopic composition of total dissolved inorganic carbon during sea ice formation and growth. Our aim was to examine factors, which initiate and control the chemistry within sea ice. Studies to date that have addressed associated processes have been conducted in field campaigns. These are almost all compromised in the conclusions that can be drawn by the lack of temporal measurements coupled with large variability associated with the spatial heterogeneity of sea ice systems (Brierley and Thomas, 2002). In this study, we employed a series of 4 m^3 tanks within an experimental ice basin facility that would enable temporal processes to be followed, and in which issues associated with spatial variability could be minimized.

Fig. 1. Experimental setting: three of the four tanks (A, B and C) are shown submerged into a larger basin 2 d after the onset of ice formation (photo: Mats Granskog).

2. MATERIALS AND METHODS

2.1. Experimental Setting

Controlled incubations of artificial seawater were set up concurrently in four 4 m^3 custom-made polyethylene tanks, which were placed in a large experimental basin (Fig. 1) at Hamburgische Schiffbau- und Versuchsanstalt (HSVA), Hamburg, Germany (http://www.hsva.de). The artificial seawater was prepared using Instant Ocean Salt (Aquarium Systems, France), with a typical ionic composition at a salinity of 35 of $[K^+] = 402$ mg L^{-1}, $[Cl^-] = 19251$ mg L^{-1}, $[Na^+] = 19757$ mg L^{-1}, $[Mg^{2+}] = 1317$ mg L^{-1}, $[Ca^{2+}] = 398$ mg L^{-1}, $[SO_4^{2-}] = 2659$ mg L^{-1} (ca. 28 mM) and $[Br^-] = 7.3$ mg L^{-1}. The seawater was enriched with nutrients to give final inorganic nutrient concentrations of 680–770 μM dissolved inorganic nitrogen (ca. 98% nitrate and 2% ammonium), 60–200 μM dissolved silicate and $\sim$ 40 μM dissolved inorganic phosphorus (G. Kattner, unpublished data). Further details of the experimental facilities used are described by Mock et al. (2002). Three of the tanks (A, B and C) were inoculated with a dense, nonaxenic Antarctic diatom culture (*Fragilariopsis cylindrus*), resulting in an initial chlorophyll a concentration of $\sim$ 11 μg L^{-1} (Mock et al., 2002) and a particulate organic carbon (POC) concentration of 500 μg C L^{-1} ($\sim$ 40 μM; unpublished data). Tank D was free of diatoms. Tanks A and B were kept at an ambient irradiance of 34 μmol photons m^{-2} s^{-1}, while the irradiance level over tank C was kept at approximately half that value. The cultures were allowed to establish in the seawater for 7 d (air temperature at 0°C), whereupon ice growth was initiated by lowering the air temperature to -10 ± 2°C. Ice formation was facilitated by briefly spraying a fine mist of distilled water over the

Table 1. Temperature range (in °C) and change in salinity-normalized C_T concentration ($s\Delta C_T$, in μmol kg^{-1}) and in $\delta^{13}C_T$ ($\Delta\delta^{13}C_T$, in ‰ VPDB) in the under-ice seawater and sackhole brine from the ice sheet.[a]

Tank	Temperature	$s\Delta C_T$	$\Delta\delta^{13}C_T$	$\delta^{13}C_{T,\,loss}$
Under-ice seawater, t = 0–17 d				
A		−37	+0.20	−20.3 ± 16.4 (6)
B		−103	+0.05	−10.1 ± 7.7 (7)
	−1.9 to −2.2			
C		−61	+0.20	−19.4 ± 12.0 (7)
D		−45	+0.35	−25.8 ± 17.1 (6)
Shallow sackhole brine, t = 8–18 d				
A	−4.2 to −5.3	−273	+0.27	−10.0 ± 6.0 (4)
B	−4.5 to −5.3	−376	+0.15	−8 ± 10 (4)
C	−4.1 to −5.7	−135	+0.56	−21.0 ± 18.5 (4)
D	−4.5 to −5.7	−284	+0.19	−8.0 ± 10.3 (4)

[a] The indicated period (t) of the elemental and isotopic change is in days after onset of ice formation. The changes were calculated relative to the initial sC_T and $\delta^{13}C_T$ measured at the beginning of the indicated period. Negative $s\Delta C_T$ indicates deviation from conservative behavior during solute expulsion from the ice matrix resulting from net C_T loss from solution. Positive isotopic change indicates ^{13}C enrichment relative to the initial $\delta^{13}C_T$. The isotopic composition of the C_T lost from solution ($\delta^{13}C_{T,\,loss}$) during the period of ice formation and growth (i.e., $s\Delta C_T$) were derived from fitting Eqn. 2 on measurements using geometric mean regression (GMR) (Ricker, 1973). The errors represent the 95% confidence interval of the GMR slope (both in ‰ VPDB), while the number of measurements is indicated in parentheses.

seawater surface. This method has been shown to result in sea ice with realistic growth trends (Giannelli et al., 2001, and references therein; Krembs et al., 2001; Mock et al., 2002). During the subsequent 18 d that freezing conditions were maintained, the thickness of the ice sheet increased steadily at a rate of 0.54 mm h^{-1} to 25–27 cm by the end of the experiment (Mock et al., 2002). The maximum temperature range through the ice sheet was from −6.7°C in its top 4 cm to −2.2°C near the ice-seawater interface (op. cit.). The seawater before freezing, and thereafter underneath the closed ice cover, was completely mixed at all times by using electric water pumps without filters. Biological activity had minimal effect on elemental and isotopic compositions during the experiment.

2.2. Sampling and Analytical Methods

Sampling and analytical results from the ice sheet and the under-ice seawater are reported with respect to the day of the onset of ice formation (t = 0). Sampling of ice brine was conducted in all tanks on t = 8, 11 and 18 d by drilling shallow (~ 7 cm) sackholes through the surface of the ice sheet and also a deeper (~ 15 cm) sackhole on the final day of the experiment (t = 18). The brine from adjacent brine channels and pockets was allowed to seep into the sackhole for 30–60 min, with the hole covered with a plastic lid (Gleitz et al., 1995).

The salinity (S) of the seawater and brine was measured with a WTW LF 191 conductivity meter (Mock et al., 2002) and is reported in p.s.u. (Practical Salinity Units).

Samples for pH measurements and for the elemental and isotopic determination of total dissolved inorganic carbon (C_T) were taken manually by immersing 20 mL plastic syringes below the surface of the seawater through openings in the ice sheet and into sackhole brines. The samples were subsequently allowed to warm up to room temperature (20 ± 2°C) in the dark (e.g., Gleitz et al., 1995) before measurement with a commercial glass electrode (Mettler Toledo Inlab 412) using a WTW pMX3200 Microprocessor pH/ION Meter. The electrode was calibrated using NBS pH buffers 6.881 and pH 9.225 (20°C) and was then allowed to stand in the first sample until a stable reading was obtained (~ 1 min). The reported values of pH_{SWS} were calculated for in situ temperature (Table 1) from the measured pH_{NBS} and C_T after calculation of total alkalinity (A_T) by keeping the C_T and A_T constant (Gleitz et al., 1995). First, the measured pH_{NBS} was converted to the seawater scale, $pH_{SWS} = \log f_H + pH_{NBS}$ (Gleitz et al., 1995), using the average of the reported values of the apparent hydrogen ion activity coefficient at S = 34.6 and S = 43.7 and 25°C in Culberson and Pytkowicz (1973), $f_H = 0.709$ and 0.730 for the under-ice seawater and sea ice brine respectively. A_T was then calculated as the sum of carbonate alkalinity, $A_C = 2[CO_3^{2-}] + [HCO_3^-]$, and the alkalinity resulting from borate, phosphate, silicate, ammonia, OH^-, and $[H^+]_{SWS}$ (Millero, 1995). Carbonate alkalinity was calculated as in UNESCO (1987), while the remaining contributions to A_T were computed from available pH, salinity and nutrient measurements (G. Kattner, unpublished data) using the relevant equations described in Millero (1995). The calculation of appropriate dissociation constants and the concentration of sulfate, fluoride and total borate (B_T) as a function of in situ salinity and temperature were also based on the equations in Millero (op. cit.), assuming conservative behavior during seawater freezing. Deviation from conservative behavior due to mineral precipitation occurs at a lower temperature than the conditions of the present experiment, e.g., < −6.3°C for sulfate by mirabilite precipitation (Marion and Farren, 1999). The resultant in situ pH_{SWS} values in the seawater are averages of duplicate pH_{NBS} measurements. Only a small number of duplicate measurements could be obtained from sackhole brines due to the limited volume of brine available. The difference between duplicate pH_{NBS} measurements was better than 0.04, but the error of the pH_{SWS} is greater due to the uncertainty in the value of f_H, which depends strongly on the electrode used. Based on f_H measurements in natural sea ice brines (Gleitz et al., 1995; D. N. Thomas and M. Gleitz, unpublished data), the uncertainty in the f_H used here can be as high as ± 0.1, especially at high salinities. Propagation of the above errors during the calculation of the in situ pH_{SWS} raises its uncertainty to 0.07 pH units.

The C_T samples were immediately filtered through glass fibre syringe filters (GF/D, 0.45 μm, WHATMAN) into prepoisoned ($HgCl_2$) 10 mL glass ampoules under nitrogen and were stored flame-sealed until analysis. The C_T was extracted from the sample by vacuum distillation as CO_2 gas after acidification with H_3PO_4 (85%) and was quantified manometrically. The CO_2 gas was then collected and its stable carbon isotopic composition ($\delta^{13}C_T$) was measured on a PDZ-EUROPA GEO 20/20 mass spectrometer. The $\delta^{13}C_T$ is reported relative to Vienna Pee Dee Bellemnite (VPDB), i.e.,

$$\delta^{13}C_{sample} = 1000\left(\frac{R_{sample}}{R_{VPDB}} - 1\right),$$

where

$$R = \frac{^{13}C}{^{12}C}.$$

The C_T concentration difference between duplicate samples from the under-ice seawater was better than 22 μmol kg^{-1} in the concentration range of 2800–4300 μmol kg^{-1}, while the reproducibility of the isotopic measurements was better than 0.2‰.

The concentration of CO_2(aq) in the seawater and sackhole brine was calculated from the in situ pH_{SWS}, the measured C_T, and the temperature- and salinity-adjusted first and second stoichiometric dissociation constants of carbonic acid, K_1^* and K_2^* (Millero, 1995), with an uncertainty of ca. 30% based on error propagation of the above parameters. The concentration of CO_2(aq) in seawater and sackhole brine at equilibrium with the atmosphere (i.e., 100% air saturation) was calculated as the product of the atmospheric pCO_2 (≈3.5 × 10^{-4} atm) and Henry's law constant, K_o, calculated for the in situ salinity and temperature using the equation found in Millero (1995).

The degree of saturation of seawater and brine with respect to carbonate minerals, calcite and aragonite ($CaCO_3$), vaterite (μ-$CaCO_3$) and ikaite ($CaCO_3 \cdot 6H_2O$) is given as

$$\Omega = \frac{[Ca^{2+}][CO_3^{2-}]}{K_{sp}^*}$$

(Millero, 1995), with quantities in brackets denoting the ion concentration in solution (in mol kg^{-1}) and K_{sp}^* = the stoichiometric equilibrium solubility product of the above minerals (in mol^2 kg^{-2}). The

concentration of calcium ions, $[Ca^{2+}]$, was derived from salinity (Millero, 1995), assuming conservative behavior during sea ice formation. Deviation from conservative behavior during the freezing of seawater is expected to occur upon gypsum precipitation at a much lower temperature (i.e., −22.2°C; Marion and Farren, 1999) than the conditions of the present experiments. The K^*_{sp} of aragonite and calcite was calculated using the equations in Mucci (1983). The K^*_{sp} of vaterite and ikaite is poorly known and was estimated from their thermodynamic equilibrium solubility product, K^o_{sp}, using the equations in Marion (2001) and Bischoff et al. (1993b) respectively as

$$K^*_{sp,vaterite} = \frac{K^o_{sp,vaterite}}{\gamma_{T,Ca^{2+}}\gamma_{T,CO_3^{2-}}}\theta^2$$

and

$$K^*_{sp,ikaite} = \frac{K^o_{sp,ikaite}}{\gamma_{T,Ca^{2+}}\gamma_{T,CO_3^{2-}}\alpha^6_{H_2O}}\theta^2,$$

where $\gamma_{T,Ca^{2+}}$ and $\gamma_{T,CO_3^{2-}}$ are total ion activity coefficients, α_{H_2O} is the activity of water in seawater and θ = (1–0.001005 S) (Millero, 1995) is a unit correction factor from mol $kg^{-1}_{H_2O}$ to mol kg^{-1} seawater. The α_{H_2O} was calculated as a function of salinity using the equation in Pytkowicz (1975). The product of the total ion activity coefficients as a function of salinity and temperature was calculated from the K^*_{sp} and K^o_{sp} of calcite (Mucci, 1983) as

$$\gamma_{T,Ca^{2+}}\gamma_{T,CO_3^{2-}} = \frac{K^o_{sp,calcite}}{K^*_{sp,calcite}}\theta^2.$$

Our calculated values differ from those reported in Mucci (1983) by 0.0006 and 0.0005 at S = 35 and S = 44 respectively, which are within the reported errors. Solid carbonates were not isolated and, thus, consistency of the data in terms of mass balance and isotopic compositions could not be verified. All calculations were done by extrapolation of the equations to in situ temperature (Table 1) and salinity for S > 40.

3. RESULTS

Sackhole brine measurements integrate chemical and isotopic changes within a variable, but unknown, volume of the ice sheet from both the surrounding and underlying ice layers. Another constraint for the application of the sackhole sampling technique is imposed by the thickness of the ice sheet, which must have grown to > 10 cm. To improve the spatial and temporal detail of the data, especially during the first 8 d of ice growth, additional sampling of the ice sheet was attempted in between sackhole sampling dates by coring with an ice auger and centrifugation of the ice sections at 1500 rpm and −5°C for 15 min to separate the brine inclusions from the solid ice matrix (Krembs et al., 2001). Analyses of these samples indicated large systematic discrepancies from sackhole measurements with respect to C_T but not $\delta^{13}C_T$ (data not shown). These are pertinent to the study of the carbonate system in brines supersaturated with respect to CO_2 and carbonate mineral phases. Furthermore, centrifugation can disturb the ice-water phase equilibrium by depressing the freezing point of seawater at the enhanced pressure generated by centrifugation (Wagner et al., 1994), which can cause melting of the centrifuged ice and dilution of the extracted brine. Consequently, coring and centrifugation of ice samples were deemed inappropriate to study brine chemistry and should be used with caution in future field biogeochemical sea ice studies.

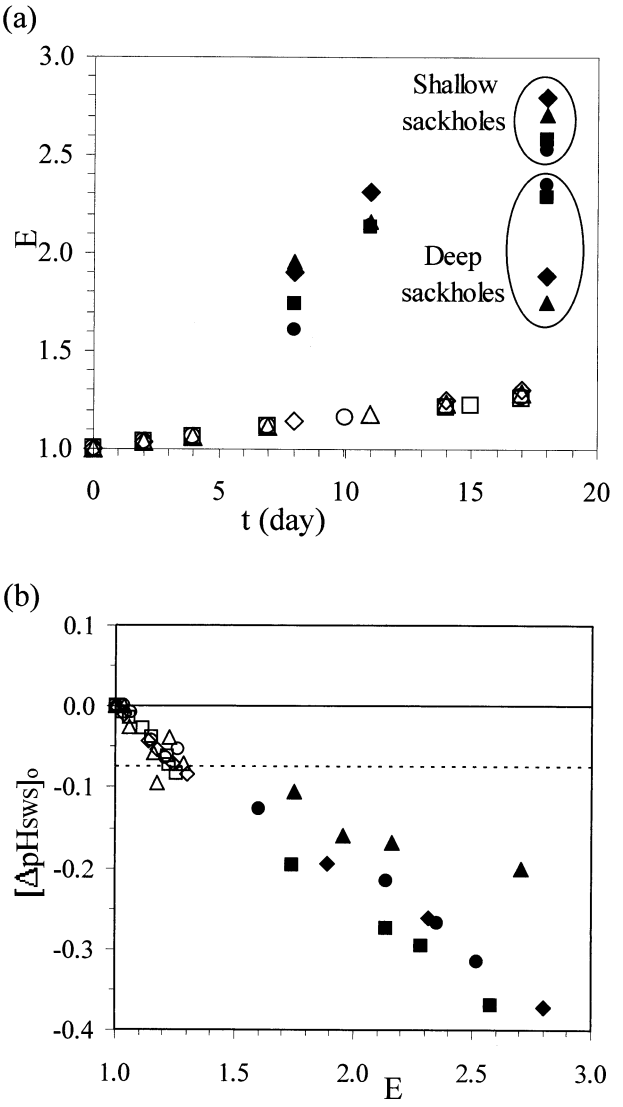

Fig. 2. a) Dissolved salt enrichment, E, in the seawater (open symbols) and sackhole brine (closed symbols) vs. time, t, in days after the onset of ice formation in tanks A (circles), B (squares), C (triangles) and D (diamonds). Sackhole brine was obtained from shallow (~ 7 cm) holes drilled into the surface of the ice sheet, while on the final day of the incubation (t = 18), brine was also obtained from ~ 15 cm deep surface holes (indicated by the encircled observations). b) pH_{SWS} change relative to $[pH_{SWS}]_o$, $[\Delta pH_{SWS}]_o$, vs. E in the seawater and sackhole brine (symbols as in top panel). The horizontal solid and dashed lines indicate, respectively, $[\Delta pH_{SWS}]_o = 0$ and maximum error estimated from $\frac{1}{2}$ of the range of duplicate pH_{NBS} measurements and the uncertainty in f_H.

3.1. Salinity and pH

The initial (t = 0) salinity (S_o) of the seawater was similar in all tanks at 33.5 ± 0.2 (n = 4). The salinity of the residual seawater and brine increased steadily with time. The salinity increase is described as the degree of dissolved salt enrichment, $E = S_t/S_o$, with S_t = salinity measured at t > 0 (Fig. 2a). The final E was 1.3 in the residual seawater in all tanks (t = 17 d) and ranged from 2.5 to 2.8 in the shallow sackhole brines and

from 1.7 to 2.4 in deep sackhole brines at the end of the experiment (t = 18 d).

Hereafter, E is used as an indicator of conservative behavior in the temperature range measured during the ice phase. The precipitation of major dissolved salts (sodium sulfate, calcium sulfate and sodium chloride), which would affect the ionic composition of the brine, is expected to occur at temperatures lower than −6.3°C that marks the onset of mirabilite ($Na_2SO_4.10H_2O$) precipitation during the freezing of seawater (Marion and Farren, 1999). This is equivalent to the minimum temperature of −6.7°C during our experiment in the top 4 cm of the ice sheet (Mock et al., 2002). Subsequently, all results are plotted against E, and it is noted that changes in the residual (under-ice) seawater and in the ice sheet were concurrent (i.e., relative to t = 0 and E = 1.0).

The initial in situ pH_{SWS} of the seawater ($[pH_{SWS}]_o$ at E = 1.0, t = 0) was 8.45 ± 0.02, 8.65 ± 0.01, 7.93 ± 0.01 and 8.71 ± 0.01 (±½ range, n = 2) in tanks A, B, C and D respectively. The pH_{SWS} of the brine and seawater was greater than 8.00 in tanks A, B and D throughout the experiment, while it was below this value in tank C. There was a systematic drop in the pH_{SWS} concurrent with the increase in E with time (E > 1.0) both in the seawater and in the brine, which was of similar magnitude in all tanks (Fig. 2b). In the residual seawater, the maximum pH_{SWS} change, $[\Delta pH_{SWS}]_o = [pH_{SWS}]_t - [pH_{SWS}]_o$, was mostly within the uncertainty of measurements and calculations (range: −0.06 to −0.08 pH units). The $[\Delta pH_{SWS}]_o$ in the brine of the ice sheet was discernible and, at its maximum in shallow sackhole brines at the end of the experiment, was higher than the concurrent change in the residual seawater and ranged from −0.20 to −0.37 pH units.

3.2. Total Dissolved Inorganic Carbon and Dissolved Carbon Dioxide

The initial concentration of total dissolved inorganic carbon in the seawater (t = 0, $[C_T]_o$) was 3030, 2940, 3440 and 2850 μmol kg^{-1} in tanks A, B, C and D respectively, and increased steadily in both the seawater and the brine. The pattern of the rise in C_T concentration with time was similar to that in E, leading to final concentrations higher than $[C_T]_o$ by a factor of 1.2–1.3 in the residual seawater and 2.4–2.7 in shallow sackhole brine respectively. Comparison of the above C_T enrichment with final E indicates the significant influence of physical concentration mechanisms on C_T during ice formation and growth. To detect possible concentration changes from processes other than physical concentration, the measured values were normalized to S_o (Gleitz et al., 1995). A correspondence with $[C_T]_o$ of salinity-normalized C_T values, $sC_T = [C_T]/E$ (Lazar and Erez, 1992), would indicate conservative behavior during ice formation. The calculated sC_T (Fig. 3) have two salient characteristics.

When all observations are taken together, they deviate from $[C_T]_o$ at E > 1.1–1.2, indicating a systematic net decrease in sC_T both in the residual seawater (Fig. 3, insets) and in the brine. In addition, the first sackhole brine measurement in each tank, which was obtained at t = 8 d due to sampling constraints imposed by ice thickness, indicated a substantial net C_T gain in the ice sheet of tanks A, B and D, and conservative C_T behavior in tank C, followed by a net decrease thereafter (t > 8 d) (Fig. 3). The decrease in sC_T was greater at higher salinities, i.e., in the ice sheet during the latter half of the experiment. Hence, the final net decrease in $[C_T]$ from the seawater, $s\Delta C_T$, was lower than that measured in the ice sheet (Table 1).

The isotopic composition of seawater C_T at t = 0 ($\delta^{13}C_{To}$) was −7.5, −6.4, −9.0 and −6.3‰ in tanks A, B, C and D respectively. There is considerable scatter in the measurements obtained during the experiment, but a tendency for ^{13}C enrichment (i.e., less negative $\delta^{13}C_T$) is evident in all tanks (Fig. 4). The isotopic change was systematic and analytically discernible in the residual seawater of tanks C and D, with a maximum relative to $\delta^{13}C_{To}$ of +0.20‰ and +0.35‰ respectively at the end of the experiment, while it was variable and mostly within the analytical precision (<± 0.20‰) in tanks A and B (Fig. 4, insets). The net C_T gain indicated by the first shallow sackhole brine measurement (i.e., t = 0–8 d; Fig. 3) was accompanied by an isotopic enrichment of up to +0.34‰. During the subsequent net C_T decrease observed in the sackhole brine (t = 8–18 d; Fig. 3), the C_T became further enriched in ^{13}C (Table 1). In summary, vertical profiles with depth in the ice sheet tend towards progressively higher net loss of C_T coupled with isotopic enrichment from the ice-seawater interface towards the top of the ice sheet.

The observed change in sC_T (Fig. 3) can be related to the isotopic change (Fig. 4) through the following mass balance:

$$\left[\frac{C_T}{E}\right]_t = \left[\frac{C_T}{E}\right]_i + \Delta[C_T]_t \quad (1)$$

$$\left[\delta^{13}C_T\frac{C_T}{E}\right]_t = \left[\delta^{13}C_T\frac{C_T}{E}\right]_i + \delta^{13}C_{T,loss}\Delta[C_T]_t \quad (2)$$

where $\delta^{13}C_{T,\,loss}$ is the isotopic composition of the product of the process, or of the combined product of processes, responsible for the sC_T and $\delta^{13}C_T$ change at time *t* relative to initial conditions (denoted with the subscript *i*). The slope, $\delta^{13}C_{T,\,loss}$, of $[\delta^{13}C_T(C_T/E)]$ vs. $\Delta[C_T]_t$ (Fig. 5) and its 95% confidence interval (Table 1). was obtained by geometric mean regression (GMR) because of errors in both variables (Ricker, 1973). The $[C_T]_o$ and $\delta^{13}C_{To}$ were used as the initial condition for the evaluation of the moderate changes that occurred in the residual seawater (Fig. 3, insets). In the ice sheet, only the net C_T decrease in the brine was adequately constrained by the existing measurements (Fig. 3) and is evaluated using the first pair of measurements obtained as an initial condition (i.e., t = 8 d).

All linear regression fits on the measurements in seawater (r^2 = 0.47 to 0.72) were statistically significant ($p \le 0.05$). Regressions on sackhole brine measurements (r^2 = 0.74–0.94) were statistically significant for tanks A (p = 0.020) and C (p = 0.043). The different number of measurements available for each group of results does not allow direct comparison between the calculated 95% confidence interval of the slopes (Table 1). This is exacerbated in the sackhole brine regressions, where the Student-t value assigned to available measurements (n = 4) was up to factor of 2 higher than that assigned to the other regressions.

The initial concentration of in situ CO_2(aq) in the seawater was 16.8, 9.6, 66.2 and 8.0 μmol kg^{-1} in tanks A, B, C and D respectively. Changes in [CO_2(aq)] in the under-ice seawater were within the uncertainty of the calculations in all tanks. In

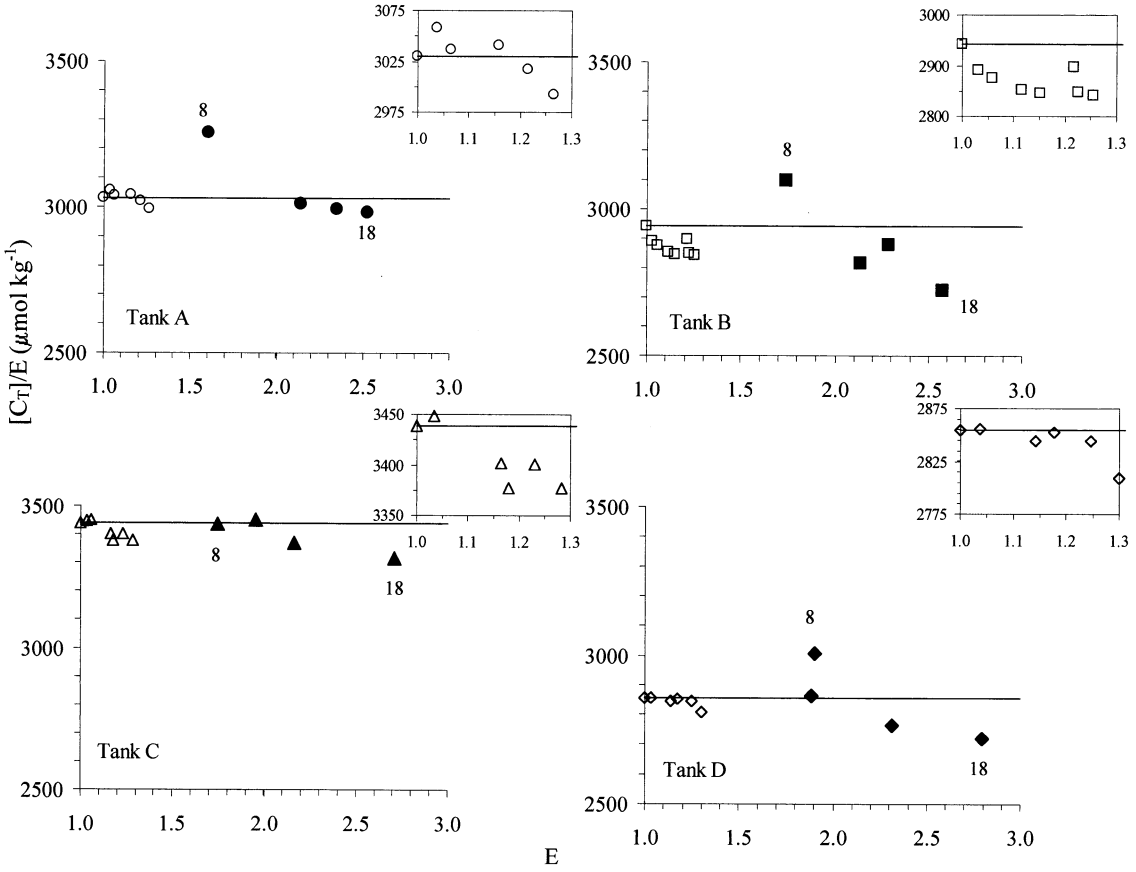

Fig. 3. Salinity-normalized total dissolved inorganic carbon, C_T/E, vs. E in the seawater and sackhole brine in tanks A, B, C and D. Insets show measurements in the seawater only. The solid line indicates $[C_T]_o$ (seawater concentration at the onset of ice formation) and the trend for conservative behavior along the path of dissolved salt enrichment during ice growth. The numbers next to symbols indicate the time in days after the onset of ice formation when brine inclusions from the ice sheet were sampled.

contrast, a systematic increase in $[CO_2(aq)]$ was observed in the ice brines to 30.7, 18.7, 104.0 and 17.1 μmol kg^{-1} in tanks A, B, C and D respectively at the end of the experiment. The equilibrium $[CO_2(aq)]$ for atmospheric $pCO_2 = 3.5 \times 10^{-4}$ atm (Marion, 2001) was calculated to decrease from 24.1 to 19.4 μmol kg^{-1} over the experimental range of temperature (-1.9 to -5.7°C) and salinity (33 to 93), indicating an overriding effect of salinity on CO_2 solubility. The percent molar ratio of in situ to equilibrium $CO_2(aq)$ was initially below the air saturation value in tanks A, B and D, while it was well above the air saturation value in tank C (Fig. 6). The $[CO_2(aq)]$ remained well below air saturation throughout ice formation and growth in the residual seawater until the end of the experiment in tanks A, B and D (data not shown). Concurrently, the $[CO_2(aq)]$ in the brine of the ice sheet tended towards and approached air saturation (tanks B and D) or supersaturation (tank A) in an apparent linear fashion with respect to E. The $[CO_2(aq)]$ in the residual seawater and in the brine of the ice sheet in tank C remained well above the air saturation value throughout the experiment.

3.3. Carbonate Mineral Equilibria

The saturation state, Ω, in the seawater and sackhole brine with respect to calcite, aragonite, vaterite and ikaite increased systematically with E by a factor of 2–3.5 to a maximum value in the sackhole brine of the ice sheet in all tanks (Fig. 7). A slight decrease in Ω by a factor of ca. 1.4–2 at an $E > 2.0$ is probably within calculation error. The initial seawater, as well as the residual seawater after ice had formed, and the sackhole brine throughout the experiment, were all well above the saturation value ($\Omega = 1$) with respect to all carbonate minerals in tanks A, B and D. In tank C, the seawater and sackhole brine were always supersaturated with respect to calcite and aragonite, while the calculated Ω with respect to vaterite and ikaite indicates undersaturation in the seawater and slight supersaturation in the sackhole brine.

4. DISCUSSION

Precipitation of $CaCO_3$ is predicted to occur in the temperature range of -1.9 to -6.7°C (Anderson and Jones, 1985; Marion, 2001). An important control on $CaCO_3$ precipitation

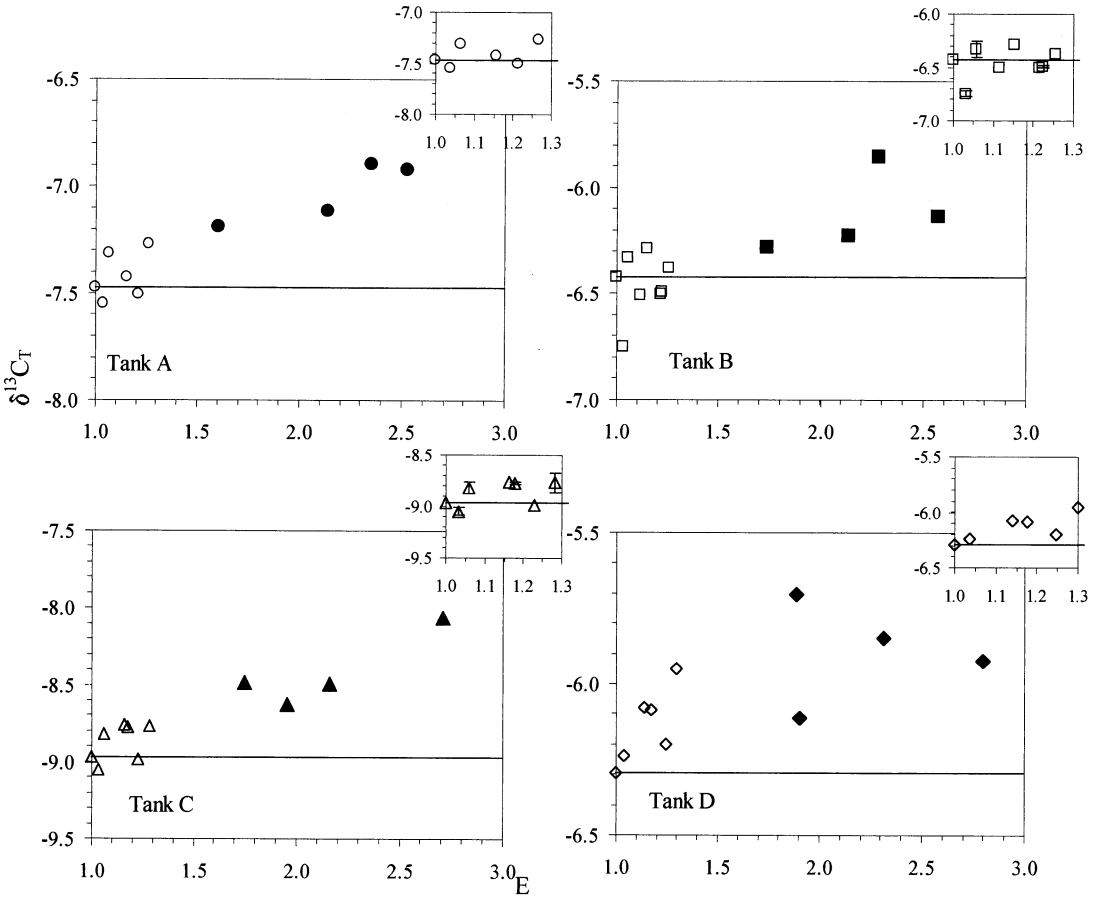

Fig. 4. $\delta^{13}C_T$ vs. E in the seawater and sackhole brine in tanks A, B, C and D. Insets show measurements in seawater only. Note the change of scale on the y-axis. The solid line indicates $\delta^{13}C_T$ at t = 0 (onset of ice phase). Error bars indicate $\pm \frac{1}{2}$ of the range (n = 2) or $\pm 1\sigma$ (n = 3) of replicate determinations.

from a solution is its saturation state (Berner, 1980). The high degree of supersaturation with respect to the anhydrous and the hydrated forms of $CaCO_3$ in the brine inclusions of the ice sheet and in the residual seawater (Fig. 7) should lead to their nucleation and precipitation as was observed previously during similar experiments for calcite and aragonite (Killawee et al., 1998). Ikaite ($CaCO_3 \cdot 6H_2O$) is the most likely $CaCO_3$ mineral to precipitate under the present experimental conditions of subzero temperatures and elevated C_T concentrations, in excess of the threshold value predicted for the initiation of ikaite precipitation at -4.5°C during the freezing of seawater (0.243 g $CaCO_3$ kg^{-1}, equivalent to $C_T \sim 2500$ μmol kg^{-1}; Marion, 2001). Nevertheless, solutions remain supersaturated throughout the experiments and $CaCO_3$ precipitation appears to be inhibited. Phosphate is a known inhibitor of the nucleation and precipitation of the anhydrous $CaCO_3$ minerals (Bischoff et al., 1993b) and was present at high concentrations up to 47μM in the under-ice seawater and 100–124 μM in the brine at the end of the experiment (G. Kattner, unpublished data). In contrast, the residual seawater of tank C was undersaturated with respect to vaterite and ikaite (Fig. 7). Direct evidence for the occurrence of $CaCO_3$ precipitates and validation of their mineralogy are not possible with the present dataset. Using the changes in the elemental and isotopic compositions of C_T during the experiment (Figs. 3, 4, and 5) and calcite and/or aragonite as case scenario, the following discussion presents indirect evidence which supports $CaCO_3$ precipitation. It is noted that diatom activity was not responsible for the changes in the elemental and isotopic compositions of C_T.

In bicarbonate-dominated solutions at pH < 9, $CaCO_3$ precipitation can result in enrichment of CO_2(aq) (Eqn. 3; after Killawee et al., 1998):

$$Ca^{2+} + 2HCO_3^- \rightarrow CaCO_3 + H_2O + CO_2 \text{ (aq or gas)} \quad (3)$$

Enrichment of CO_2(aq) was evident in the brine of all the tanks as a systematic rise in the in situ concentration by a factor of 1.6–2.1 at the end of the experiment relative to the initial [CO_2(aq)] in the seawater. The CO_2(aq) enrichment of the brine could also have preceded $CaCO_3$ precipitation, resulting from changes in dissolved carbonate equilibria during dissolved salt enrichment at low temperature as reflected by the pH decrease (Fig. 2b). In this case, the overall reaction resulting from this shift in the dissociation constants in a bicarbonate-dominated solution can be described as follows:

$$H^+ + HCO_3^- \rightarrow H_2O + CO_2 \text{ (aq or gas)} \quad (4)$$

As indicated in Eqns. 3 and 4, both the above processes can

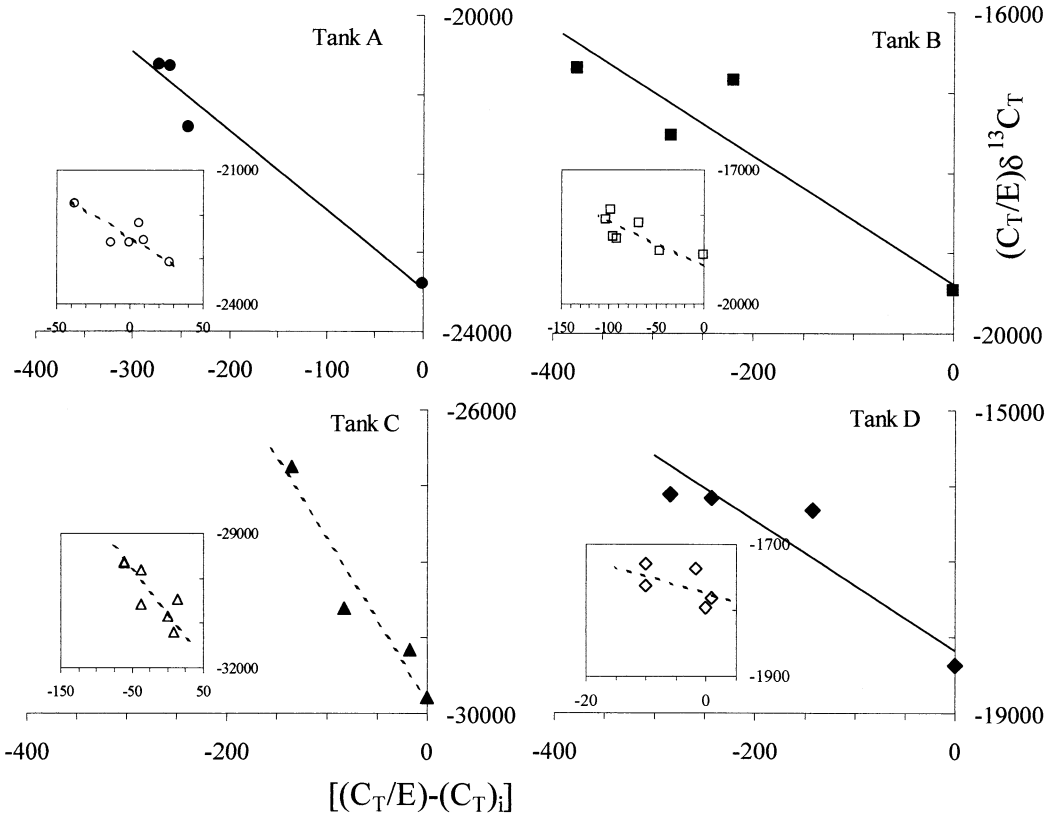

Fig. 5. $\left[\frac{C_T}{E}\right]\delta^{13}C_T$ versus $\left[\frac{C_T}{E}\right]_t - \left[\frac{C_T}{E}\right]_i$ in the sackhole brine and seawater (insets) in tanks A, B, C and D (note the change of scale but same range on the y-axis). Solid and dashed lines indicate geometric mean regression fit of Eqn. 2.

lead to degassing of dissolved CO_2. Since the ice sheets and the residual seawater have limited exchange with the atmosphere, CO_2 degassing will occur when gas bubbles are formed within the brine as well as when isolated brine inclusions are in contact with gas bubbles initially formed near the ice-seawater interface and subsequently trapped within the growing ice sheet. Gas bubble formation begins when a critical supersaturation value is exceeded and is facilitated by turbulence in the under-ice seawater and the occurrence of nucleation sites, i.e., preexisting or authigenic particles (Killawee et al., 1998). In terms of constraints imposed by critical CO_2(aq) supersaturation, the potential for CO_2 degassing into gas bubbles is limited to the highest supersaturation levels that developed in tanks A and C (Fig. 6). Gas bubbles were observed in tank A and were more abundant towards the top section of the ice sheet (Mock et al., 2002).

Degassing of CO_2 can be distinguished from $CaCO_3$ precipitation on the basis of the distinct isotope effect that each process has on the C_T pool. The magnitude of the isotope effect depends on temperature, as well as the extent of kinetic and equilibrium isotopic fractionation amongst the gaseous, aqueous and solid phases, including the precipitating $CaCO_3$ mineral (e.g., Aharon, 1988). The extent of isotopic fractionation (i.e., ^{13}C-enrichment or depletion) of species *i* relative to species *j* is described by the per mil isotope fractionation factor $\varepsilon_{i\text{-}j} = 1000\ (\alpha_{i-j} - 1)$, where $\alpha_{i-j} = (R_i/R_j)$ is the isotope fractionation factor and R is the ^{13}C to ^{12}C ratio. The partitioning of stable carbon isotopes amongst the gaseous, dissolved and solid phases is governed by thermodynamic equilibrium (Romanek et al., 1992; Zhang et al., 1995) or can be kinetically controlled by the different diffusivities of ^{12}C and ^{13}C across the gas-liquid and solid-liquid interfaces (Turner, 1982; Stiller et al., 1985; Aharon, 1988). At isotopic equilibrium and 0°C, evolved CO_2 will be ^{13}C-depleted relative to HCO_3^- by $(\varepsilon_{CO_2(g)-HCO_3^-})_{eq} = -10.7‰$ (Zhang et al., 1995), while the precipitated $CaCO_3$ will be ^{13}C-enriched by $(\varepsilon_{calcite-HCO_3^-})_{eq} = +1.2‰$ and $(\varepsilon_{aragonite-HCO_3^-})_{eq} = +3.1‰$ as calculated from the equilibrium fractionation factor of calcite and aragonite, respectively, relative to gaseous CO_2 (Romanek et al., 1992) and the equilibrium fractionation factors of C_T species relative to gaseous CO_2 as given in Zhang et al. (1995). Kinetic effects during CO_2 gas exchange result in more negative isotopic fractionation between gaseous CO_2 and dissolved carbonate species than at isotopic equilibrium. The kinetic isotopic fractionation between degassed CO_2 and the C_T in Dead Sea brine (pH = 6.0–6.2) was measured to be $-16.2 \pm 0.3‰$ at 24°C (Barkan et al., 2001) and $-19.4‰$ at 45°C (Stiller et al., 1985). The theoretical maximum diffusion-controlled kinetic fractionation between gaseous CO_2 and

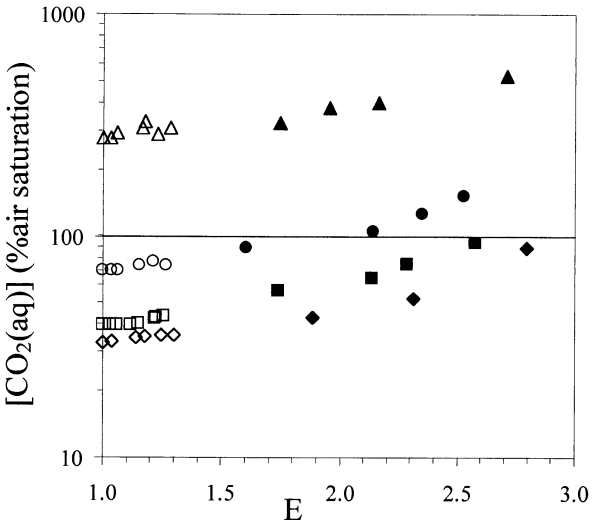

Fig. 6. The concentration of CO_2(aq), expressed as percent molar ratio relative to its concentration at equilibrium with air (% air saturation) vs. E in the seawater (open symbols) and sackhole brine (closed symbols) in tanks A (circles), B (squares), C (triangles) and D (diamonds). The solid line indicates 100%air saturation.

CO_2 (aq), $(\varepsilon_{CO_2(g)-CO_2(aq)})_{kin} = -11.2‰$ (Stiller et al., 1985), can be superimposed on the temperature-dependent equilibrium fractionation between CO_2(aq) and HCO_3^-, $(\varepsilon_{CO_2(aq)-HCO_3^-})_{eq}(-12.0‰$; Zhang et al., 1995), leading to an $(\varepsilon_{CO_2(aq)-HCO_3^-})_{kin} = -23.1‰$ between degassed CO_2 and HCO_3^- at 0°C. Similarly, a kinetic isotope effect during precipitation will lead to more ^{13}C-depleted isotopic fractionation between $CaCO_3$ and HCO_3^- than at isotopic equilibrium (see above) and can be a function of precipitation rate (Turner, 1982).

The above fractionation factors indicate that CO_2 degassing alone of bicarbonate-dominated solutions will result in ^{13}C-enrichment of the C_T remaining in solution, whereas equilibrium fractionation resulting from $CaCO_3$ precipitation alone will have the opposite effect on $\delta^{13}C_T$. When $CaCO_3$ precipitation and CO_2 degassing remove C_T from solution simultaneously, the isotopic fractionation between the C_T lost from solution to the gaseous and solid phases and the C_T remaining in solution (measured) is given by $\varepsilon_{loss} = \varepsilon_{C_T,loss-C_T} = f_{degassing}\ \varepsilon_{degassing} + f_{precipitation}\ \varepsilon_{precipitation}$, where $f_{degassing}$ and $f_{precipitation}$ represent the fractional contribution of each process to the C_T loss from solution, and $\varepsilon_{degassing}$ and $\varepsilon_{precipitation}$ are their isotope fractionation factors (after Barkan et al., 2001). When the precipitation reaction (i.e., Eqn. 3) proceeds to CO_2 degassing without intermediate build-up of CO_2(aq), one mole CO_2 will be degassed for every mole of $CaCO_3$ precipitated, leading to two mole of C_T lost from solution, such as in systems open to exchange with the atmosphere (Usdowski et al., 1979; Stiller et al., 1985). In this case, $f_{degassing} = f_{precipitation} = 0.5$, and ε_{loss} is calculated to be $-3.8‰$ and $-4.7‰$ for aragonite and calcite precipitation at isotopic equilibrium. The ε_{loss} will be more negative than at isotopic equilibrium, if the isotope effects of both these processes are kinetically controlled. For example, using the maximum $(\varepsilon_{CO_2(g)-CO_2(aq)})_{kin}$ at 0°C calculated above and an $(\varepsilon_{CaCO_3-HCO_3^-})_{kin} \sim 0‰$ (e.g., Turner, 1982), an $\varepsilon_{loss} = -11.6‰$ can be calculated. When partial CO_2 degassing occurs during precipitation, as has been observed in ice systems restricted from exchange with the atmosphere (Killawee et al., 1998), the fractional contribution of gas exchange to the C_T lost from the solution will decrease and, conversely, the fractional contribution of $CaCO_3$ precipitation will increase, i.e., $0 \le f_{degassing} < 0.5$ and $0.5 < f_{precipitation} \le 1$. Therefore, the less extensive the degassing, the more ε_{loss} will approach $\varepsilon_{precipitation} \sim \varepsilon_{CaCO3-HCO_3^-}$.

By combining the equations that define $\delta^{13}C$ (given in section 2.2) as well as ε and ε_{loss} given above, ε_{loss}can be transformed to the δ notation as

$$\varepsilon_{loss} = \frac{\delta^{13}C_{T,loss} - \delta^{13}C_T}{1 + \frac{\delta^{13}C_T}{1000}}.$$

The slope of Eqn. 2 represents, to a first approximation, a regression-fitted average of the isotopic composition of the C_T removed from solution during ice formation. The fitted $\delta^{13}C_{T,\,loss}$ (Table 1) can be expressed as an apparent ε_{loss} ($\varepsilon_{loss,\,app}$) relative to the initial $[\delta^{13}C_T]_i$ (Eqn. 5):

$$\varepsilon_{loss,app} = \frac{\delta^{13}C_{T,loss} - [\delta^{13}C_T]_i}{1 + \frac{[\delta^{13}C_T]_i}{1000}} \quad (5)$$

The calculated $\varepsilon_{loss,\,app}$ (Fig. 8) can be compared with the theoretical per mil isotope fractionation factors above, considering that, in the pH range of the experiments, the majority of C_T (73–93%) was present as HCO_3^-, and, hence, $\delta^{13}C_b \sim \delta^{13}C_T$. It is noted that the uncertainty in the $\varepsilon_{loss,\,app}$ values calculated for the residual seawater and sackhole brine is as large as the error of the regression slopes (Table 1; see also section 4.2) and is not included in Figure 8 for clarity.

From the fractionation factors for CO_2 degassing and $CaCO_3$ precipitation, it can be seen that the distribution of calculated $\varepsilon_{loss,\,app}$ in all but one of the tanks falls between the theoretical values for the two processes (Fig. 8). The exception is the $\varepsilon_{loss,\,app}$ from the under-ice seawater in tank D, which is strongly ^{13}C-depleted and appears consistent with the extreme isotope discrimination under kinetically controlled degassing. This is the only evidence for kinetic isotope effects but is associated with a large uncertainty (e.g., Table 1), while the rest of the $\varepsilon_{loss,\,app}$ values are consistent with equilibrium isotope fractionation effects (Fig. 8). Furthermore, where mineral supersaturation was greatest (Fig. 7), the occurrence of $CaCO_3$ precipitation appears to become prominent in the brine. For example, $CaCO_3$ precipitation appears to be quantitatively as important as CO_2 degassing in the ice sheet (i.e., $\varepsilon_{loss,\,app}$ is close to the theoretical ε_{loss} computed for $f_{degassing} = f_{precipitation} = 0.5$), if both processes proceeded to isotopic equilibrium.

The largest decrease in the concentration of C_T was observed within the ice sheet (Table 1), which essentially operates as a closed system and presents the greatest interest in terms of processes related to sea ice formation. Based on the above discussion (Fig. 8), the observed elemental and isotopic C_T changes in the ice sheet can be treated as the result of two Rayleigh distillation processes occurring simultaneously. To this end, the Rayleigh-type distillation equation of Barkan et al.

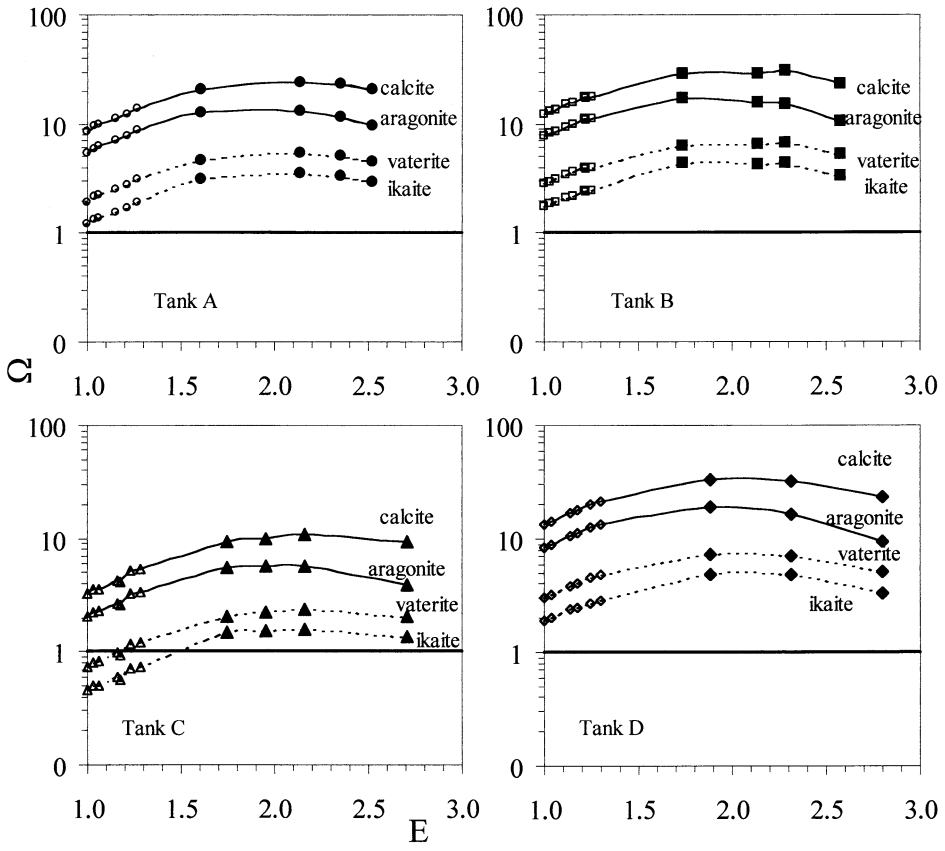

Fig. 7. Degree of saturation, Ω, vs. E with respect to carbonate minerals calcite, aragonite, vaterite and ikaite in the seawater (open symbols) and sackhole brine (closed symbols) in tanks A, B, C and D.

(2001) (Eqn. 6) can be used, with $f_{degassing}$, $f_{precipitation}$, $\varepsilon_{degassing}$ and $\varepsilon_{precipitation}$ as defined previously and subscript *i* indicating initial conditions.

$$\delta^{13}C_T = \delta^{13}C_{T,i} + (f_{degassing}\,\varepsilon_{degassing} + f_{precipitation}\,\varepsilon_{precipitation}) \ln \frac{[C_T]}{[C_T]_i} \quad (6)$$

In each tank, the distribution of results from this model is non linear (Fig. 9), consistent with a varying contribution of $CaCO_3$ precipitation and CO_2 degassing during the experiment. In young ice sheets, a varying contribution of these two processes can arise if they are decoupled initially up to a point when the occurrence of one process leads to the onset of the other at a later stage of ice growth. For example, CO_2 degassing can be initiated after accumulation of CO_2(aq) as a by-product of $CaCO_3$ precipitation (i.e., Eqn. 3) above a critical CO_2(aq) supersaturation level (e.g., Killawee et al., 1998). Given this implication, exact quantitative analysis is not possible by fitting Eqn. 6 above on the present limited data set, but only a few qualitative points can be raised. In the following discussion, calcite precipitation and isotopic equilibrium are used as reference points and case scenario. The observations from the upper 7 cm of the ice sheet in tanks A, B and D fall between the trends predicted for calcite precipitation alone and precipitation coupled with CO_2 degassing with equal fractional contribution for each process (Fig. 9). In other words, carbonate precipitation in tanks A, B and D appears to be coupled with partial CO_2 degassing. In contrast, the observations from tank C are consistent with CO_2 degassing alone (Fig. 9). The tendency for greater CO_2 degassing in tank C is consistent with the higher CO_2(aq) supersaturation in this tank compared with the other three tanks (Fig. 6). Similarly, $CaCO_3$ precipitation in tanks A, B and D (Fig. 9) reflects the higher $CaCO_3$ supersaturation of the seawater and brines in these tanks than in tank C, especially if ikaite is the solubility controlling mineral phase in the brine of the ice sheet (Fig. 7).

5. OVERVIEW AND IMPLICATIONS FOR SEA ICE SYSTEMS

The experimental results and interpretations indicate that the decline in sC_T and its isotopic enrichment in the ice sheet during the present experiment are consistent with $CaCO_3$ precipitation and CO_2 degassing. The effect of these processes in situ in the ice sheet became evident in the C_T pool eight days after the onset of ice formation (Fig. 3). The amount of CO_2 degassing within the ice sheet appears to have been greater than the $f_{degassing} \approx 0.04$ previously measured during the freezing of low ionic strength bicarbonate solutions (Killawee et al., 1998), which would have an inconsequential isotope effect. The higher extent of CO_2 degassing within the ice sheet suggested by the

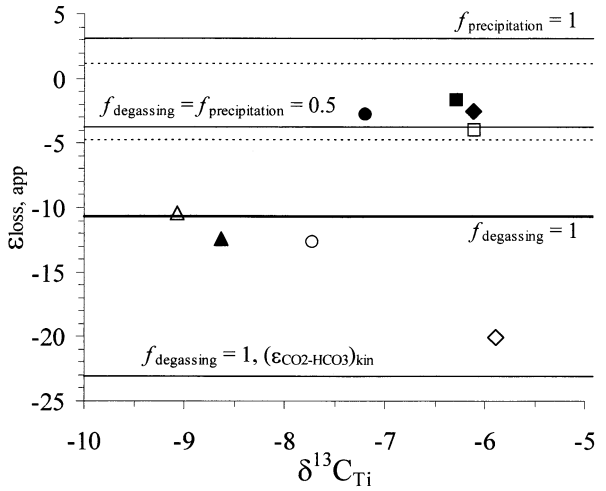

Fig. 8. Apparent per mil carbon isotope fractionation between the C_T lost from solution and the C_T remaining in solution, $\varepsilon_{loss,\ app}$ (Eqn. 5; in ‰), during ice formation and growth versus the initial isotopic composition of C_T, $[\delta^{13}C_T]_i$, in the seawater (open symbols) and sackhole brine (closed symbols) in tanks A (circles), B (squares), C (triangles) and D (diamonds). The horizontal lines indicate theoretical per mil isotope fractionation factors for CO_2 degassing only ($f_{degassing} = 1$, hence $f_{precipitation} = 0$), calcite (solid line) or aragonite (dashed line) precipitation only ($f_{precipitation} = 1$, hence $f_{degassing} = 0$), and calcite (solid line) or aragonite (dashed line) precipitation coupled with CO_2 degassing and equal fractional contribution to the C_T loss from solution ($f_{degassing} = f_{precipitation} = 0.5$), using the theoretical equilibrium per mil isotope fractionation factors of the product(s) of these processes relative to HCO_3^- at 0°C. The maximum isotope fractionation factor calculated for kinetically controlled CO_2 degassing (see text for calculation details) is also indicated.

present data (e.g., Tank C; Fig. 9) can be attributable to the high ionic strength of the present solutions and the occurrence of brine pockets within the ice sheet by comparison to the minimal porosity of ice formed from low ionic strength water. Further, the salinity effect on the solubility of CO_2 (i.e., decrease in solubility with increasing S) overrides the temperature effect (i.e., increase in solubility with decreasing temperature) and facilitates rapid attainment of CO_2 saturation or supersaturation in the sea ice brines, which can lead to enhanced rates of degassing relative to low ionic strength solutions. The saturation state of the brines with respect to CO_2(aq) was not alleviated but, instead, increased steadily until the end of the experiment (Fig. 6). This is consistent with a rate of degassing which was much slower than the rate of CO_2(aq) accumulation either via $CaCO_3$ precipitation (Eqn. 3), or by bicarbonate dehydration to CO_2(aq) (Eqn. 4), which is superimposed on the net decrease of the thermodynamic solubility of CO_2 in the cryogenic, high salinity brines.

$CaCO_3$ precipitation is expected under conditions of natural sea ice formation (Gitterman, 1937; Anderson and Jones, 1985; Marion, 2001).The extent to which CO_2 degassing and $CaCO_3$ precipitation will proceed within natural sea ice depends on the development of a mineral and gas supersaturation conducive to these processes and, hence, on the C_T concentration and pH of the source seawater. While the pH of the seawater in our experiments can be considered to be representative of the pH range encountered in the aquatic environment, the initial seawater C_T concentration (2800–3500 μmol kg^{-1}) is not typical of open, surface ocean waters (~2000 μmol kg^{-1}), where natural sea ice forms.

During natural sea ice formation, biological assemblages are readily incorporated into the ice, and their continual growth can cause chemical and isotope effects, most notably via photosynthesis by sea ice micro-algae (Gleitz et al., 1995; Gleitz et al., 1996; Gibson and Trull, 1999; Krembs et al., 2001; Kennedy et al., 2002; Thomas and Papadimitriou, 2003). It can be expected that continuing photosynthesis within natural sea ice over much longer than experimental time scales will lead to biotic effects being superimposed on the abiotic chemical and isotopic changes in the C_T pool of the brine that may occur during the initial stages of ice formation. Existing field observations consist of spatial measurements, commonly derived during or after periods of intense biologic activity within the sea ice and, hence, are overridden by its effects.

The above can explain the lack of evidence for in situ $CaCO_3$ precipitation in natural sea ice habitats based on bulk ice and brine chemistry (e.g., Anderson and Jones, 1985; Gleitz et al., 1995). Secondary $CaCO_3$ mineral deposits and inclusions are typical in glacial, subglacial, proglacial and supraglacial environments (Aharon, 1988; Clark and Lauriol, 1992; Killawee et al., 1998; Omelon et al., 2001; Grasby, 2003). Based on the results of the present experiment, direct investigation in natural sea ice environments is clearly required to document the absence of $CaCO_3$ authigenesis despite favorable thermodynamic

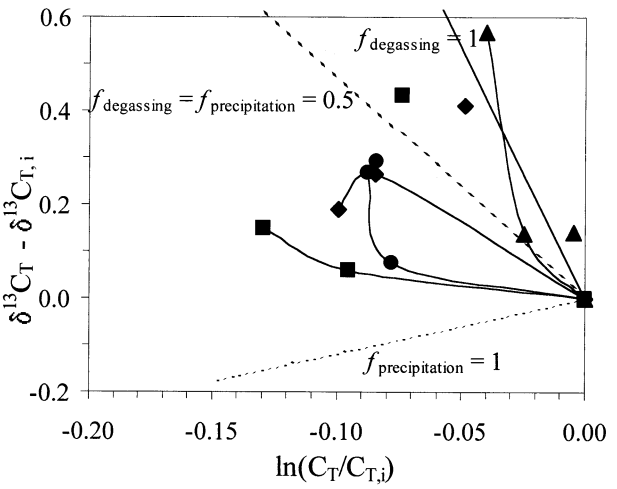

Fig. 9. $\delta^{13}C_T$-$\delta^{13}C_{T,\ i}$ vs. $\ln(C_T/C_{T,\ i})$, with subscript *i* representing initial values (i.e., measurements taken on t = 8 d) relative to which subsequent $\delta^{13}C_T$ and C_T measurements in sackhole brines are evaluated using the Rayleigh-type distillation equation (Eqn. 6) in tanks A (circles), B (squares), C (triangles), and D (diamonds). Linked symbols indicate measurements in shallow sackhole brines; it is noted that these curves do not indicate functional relationship and serve only illustration purposes. Free symbols indicate measurements in deep sackhole brines taken on the final day of the experiment (t = 18 d). Solid and dashed straight lines indicate the trends predicted for CO_2 degassing only ($f_{degassing} = 1$, hence $f_{precipitation} = 0$), calcite precipitation only ($f_{precipitation} = 1$, hence $f_{degassing} = 0$), and coupled calcite precipitation and CO_2 degassing with equal fractional contribution to the C_T loss from solution ($f_{degassing} = f_{precipitation} = 0.5$), using theoretical equilibrium per mil isotope fractionation factors of the product of these processes relative to HCO_3^- at 0°C.

conditions and, if it occurs, as shown in other glacial systems, to examine the fate of the precipitates as sea ice ages and melts.

Acknowledgments—We would like to thank K.-U. Evers and the ice tank crew of HSVA for their hospitality and technical support during the experiments in the ARTECLAB. Excellent technical assistance was also provided by Erika Allhusen during the preparation of the experiment, and by Paul Kennedy with the mass spectrometer. The research and activities at HSVA were funded by the EU Human Potential and Mobility program through contract HPRI-CI-1999-00035 and by a small NERC research grant. D. N. Thomas is grateful to the Hanse Institute of Advance Study and the Royal Society for support. We thank Prof. A. Mucci and three anonymous reviewers for their insightful comments on the manuscript.

Associate editor: A. Mucci

REFERENCES

Aharon P. (1988) Oxygen, carbon and U-series isotopes of aragonites from Vestfold Hills, Antarctica: Clues to geochemical processes in subglacial environments. *Geochim. Cosmochim. Acta* **52,** 2321–2331.

Anderson L. G. and Jones E. P. (1985) Measurements of total alkalinity, calcium and sulphate in natural sea ice. *J. Geophys. Res.* **90,** 9194–9198.

Barkan E., Luz B., and Lazar B. (2001) Dynamics of the carbon dioxide system in the Dead Sea. *Geochim. Cosmochim. Acta* **65,** 355–368.

Berner R. A. (1980) *Early Diagenesis*: *A Theoretical Approach*. Princeton University Press.

Bischoff J. L., Stine S., Rosenbauer R. J., Fitzpatrick J. A., and Stafford T. W., Jr.. (1993a) Ikaite precipitation by mixing of shoreline springs and lake water, Mono Lake, California, USA. *Geochim. Cosmochim. Acta* **57,** 3855–3865.

Bischoff J. L., Fitzpatrick J. A., and Rosenbauer R. J. (1993b) The solubility and stabilization of ikaite ($CaCO_3 \cdot 6H_2O$) from 0° to 25°C: Environmental and paleaoclimatic implications for thinolite tufa. *J. Geol.* **101,** 21–33.

Brierley A. S. and Thomas D. N. (2002) The ecology of Southern Ocean pack ice. *Adv. in Mar. Biol.* **43,** 171–278.

Clark I. D. and Lauriol B. (1992) Kinetic enrichment of stable isotopes in cryogenic calcites. *Chem. Geol.* **102,** 217–228.

Comiso J. C. (2003) Large-scale characteristics and variability of the global sea ice cover. In *Sea Ice—An Introduction to Its Physics, Chemistry, Biology and Geology* (eds. D. N. Thomas and G. S. Dieckmann), pp. 112–142. Blackwell Science.

Culberson C. and Pytkowicz R. M. (1973) Ionization of water in seawater. *Mar. Chem.* **1,** 309–316.

Dieckmann G. S. and Hellmer H. H. (2003) The importance of sea ice –an overview. In *Sea Ice—An Introduction to Its Physics, Chemistry, Biology and Geology* (eds. D. N. Thomas and G. S. Dieckmann), pp. 1–21. Blackwell Science.

Eicken H. (2003) From the microscopic, to the macroscopic, to the regional scale: Growth, microstructure and the properties of sea ice. In *Sea Ice—An Introduction to Its Physics, Chemistry, Biology and Geology* (eds. D. N. Thomas and G. S. Dieckmann), pp. 22–81. Blackwell Science.

Fairchild I. J., Bradby L., and Spiro B. (1993) Carbonate diagenesis in ice. *Geology* **21,** 901–904.

Giannelli V., Thomas D. N., Haas C., Kattner G., Kennedy H., and Dieckmann G. S. (2001) Behaviour of dissolved organic matter and inorganic nutrients during experimental sea ice formation. *Ann. Glaciol.* **33,** 317–321.

Gibson J. A. E. and Trull T. W. (1999) Ann. cycle of fCO_2 under sea-ice and in open water in Prydz Bay, East Antarctica. *Mar. Chem.* **66,** 187–200.

Gitterman K. E. (1937) Thermal analysis of seawater. *CRREL TL,* Vol. 287. USACRREL.

Gleitz M., Rutgers v. d. Loeff M, Thomas DN, Dieckmann GS and Millero FJ. (1995) Comparison of summer and winter inorganic carbon and nutrient concentrations in Antarctic sea ice brine. *Mar. Chem.* **51,** 81–91.

Gleitz M., Kukert H., Riebesell U., and Dieckmann G. S. (1996) Carbon acquisition and growth of Antarctic sea ice diatoms in closed bottle incubations. *Mar. Ecol. Prog. Ser.* **135,** 169–177.

Grasby S. E. (2003) Naturally precipitating vaterite (μ-$CaCO_3$) spheres: Unusual carbonates formed in an extreme environment. *Geochim. Cosmochim. Acta* **67,** 1659–1666.

Kennedy H., Thomas D. N., Kattner G., Haas C., and Dieckmann G. S. (2002) Particulate organic matter in Antarctic summer sea ice: Concentration and stable isotopic composition. *Mar. Ecol. Prog. Ser.* **238,** 1–13.

Killawee J. A., Fairchild I. J., Tison J.-L., Janssens L., and Lorrain R. (1998) Segregation of solutes and gases in experimental freezing of dilute solutions: Implications for natural glacial systems. *Geochim. Cosmochim. Acta* **62,** 3637–3655.

Krembs C., Mock T., and Gradinger R. (2001) A mesocosm study of physical-biological interactions in artificial sea-ice: Effect of brine channel surface evolution and brine movement on algal biomass. *Polar Biol.* **24,** 356–364.

Kühl M., Glud R. N., Borum J., Roberts R., and Rysgaard S. (2001) Photosynthetic performance of surface-associated algae below sea-ice as measured with a pulse-amplitude-modulated (PAM) fluorometer and O_2 microsensors. *Mar. Ecol. Prog. Ser.* **223,** 1–14.

Lazar B., Starinsky A., Katz A., and Sass E. (1983) The carbonate system in hypersaline solutions: Alkalinity and $CaCO_3$ solubility of evaporated seawater. *Limnol. Oceanogr.* **28,** 978–986.

Lazar B. and Erez J. (1992) Carbon geochemistry of marine-derived brines: I. ^{13}C depletion due to intense photosynthesis. *Geochim. Cosmochim. Acta* **56,** 335–345.

Lizotte M. P. (2001) The contributions of sea ice algae to Antarctic marine primary production. *Am. Zool.* **41,** 57–73.

Marion G. M. (2001) Carbonate mineral solubility at low temperatures in the Na-K-Mg-Ca-H-Cl-SO_4-OH-HCO_3-CO_3-CO_2-H_2O system. *Geochim. Cosmochim. Acta* **65,** 1883–1896.

Marion G. M. and Farren R. E. (1999) Mineral solubilities in the Na-K-Mg-Ca-Cl-SO_4-H_2O system: A re-evaluation of the sulfate chemistry in the Spencer-Moller-Weare model. *Geochim. Cosmochim. Acta* **63,** 1305–1318.

Millero F. J. (1995) Thermodynamics of the carbon dioxide system in the oceans. *Geochim. Cosmochim. Acta* **59,** 661–677.

Mock T., Dieckmann G. S., Haas C., Krell A., Tison J.-L., Belem A. L., Papadimitriou S., and Thomas D. N. (2002) Micro-optodes in sea ice: A new approach to investigate oxygen dynamics during sea ice formation. *Aquat. Microbial Ecol.* **29,** 297–306.

Mucci A. (1983) The solubility of calcite and aragonite in seawater at various salinities, temperatures, and one atmosphere total pressure. *Am. J. Sci.* **283,** 780–799.

Omelon C. R., Pollard W. H., and Marion G. M. (2001) Seasonal formation of ikaite ($CaCO_3 \cdot 6H_2O$) in saline spring discharge at Expedition Fiord, Canadian High Arctic: Assessing conditional constraints for natural crystal growth. *Geochim. Cosmochim. Acta* **65,** 1429–1437.

Pytkowicz R. M. (1975) Activity coefficients of bicarbonates and carbonates in seawater. *Limnol. Oceanogr.* **20,** 971–975.

Ricker W. E. (1973) Linear regressions in fishery research. *J. Fish. Res. Board Can.* **30,** 409–434.

Romanek C. S., Grossman E. L., and Morse JW. (1992) Carbon isotopic fractionation in synthetic aragonite and calcite: Effects of temperature and precipitation rate. *Geochim. Cosmochim. Acta* **56,** 419–430.

Stiller M., Rounick J. S., and Shasha S. (1985) Extreme carbon-isotope enrichment in evaporating brines. *Nature* **316,** 434–435.

Thomas D. N. and Dieckmann G. S. (2002a) Antarctic sea ice –a habitat for extremophiles. *Science* **295,** 641–644.

Thomas D. N. and Dieckmann G. S. (2002b) Biogeochemistry of. Antarctic sea ice. *Oceanogr. Mar. Biol. Annu. Rev.* **40,** 143–169.

Thomas D. N. and Papadimitriou S. (2003) Biogeochemistry of sea ice. In *Sea Ice—An Introduction to Its Physics, Chemistry, Biology and Geology* (eds. D. N. Thomas and G. S. Dieckmann), pp. 267–302. Blackwell Science.

Turner J. V. (1982) Kinetic fractionation of carbon-13 during calcium carbonate precipitation. *Geochim. Cosmochim. Acta* **46,** 1183–1191.

UNESCO. (1987) Thermodynamics of the carbon dioxide system in seawater. Report by the carbon dioxide sub-panel of the joint panel

on oceanographic tables and standards. UNESCO technical papers in marine science, 51.

Usdowski E., Hoefs J., and Menschel G. (1979) Relationship between ^{13}C and ^{18}O fractionation and changes in major element composition in a recent calcite-depositing spring –a model of chemical variations with inorganic $CaCO_3$ precipitation. *Earth Planet. Sci. Lett.* **42,** 267–276.

Wagner W., Saul A., and Pruss A. (1994) International equations for the pressure along the melting and along the sublimation curve of ordinary water substance. *J. Phys. Chem. Ref. Data* **23,** 515–525.

Zhang J., Quay P. D., and Wilbur D. O. (1995) Carbon isotope fractionation during gas-water exchange and dissolution of CO_2. *Geochim. Cosmochim. Acta* **59,** 107–114.